Ga-67 Imaging with Scintillation Camera: The Selection of Collimator

Hiroyuki Shinohara and Yasushi Koga

Fujigaoka Hospital, Showa University Fujigaoka, Midori-ku, Yokohama-shi, 227 Japan

Ga-67 scintiphotos made with 300 and 360 keV collimators (LFOV) were compared to determine which collimator performed better. One target was a modified Rollo phantom; the other an Anger focal photon-deficient phantom. Three energy windows were used to bracket the 93-, 185-, and 300-keV peaks of Ga-67. The MTF and contrast efficiency functions of the 360 keV collimator were found higher than those of the 300 keV; on the other hand, the latter one was graded higher by a performance index. The modified Rollo phantom images were studied by four observers to determine how well photon-deficient lesions could be seen. From their findings the "lesion-detecting ability" of each collimator was calculated—i.e., the number of lesions with decreased activity detected divided by the number actually present in the phantom. This quotient was found higher for the 360 keV than for the other one. The advantage of the 360 keV collimator was also suggested by a study of clinical Ga-67 scintigrams of a liver with focal defects.

J Nucl Med 22: 169–176, 1981

Gallium-67 is recognized as a useful tumor-seeking agent, not only for the detection of malignant tumors, but also in the diagnosis of benign disease. Rectilinear scanners have been used for Ga-67 imaging, but with improvements in the performance of the scintillation camera, the latter is becoming predominant. Recent cameras have three energy windows and can detect the 93-, 185-, and 300-keV peaks of Ga-67 separately, providing better photon density and restriction of the scatter fraction. ROC analysis on the Ga-67 images made with (a) a dual 5-in. rectilinear scanner with a single window covering the 93- and 185-keV peaks, and (b) a large-field camera with triple window, shows the latter's performance to be better (*1, 2*).

There are many factors affecting Ga-67 imaging with a scintillation camera, but the choice of collimator is one of the most important and is the only one that the user can readily change. Although several kinds of parallel-hole, low-energy collimators are available commercially, those designed for higher energies are relatively scarce. Moreover the collimator recommended by one manufacturer does not always agree with that of another. It is therefore desirable for a user to have an evaluation method useful in the selection of a collimator. As a first step in this study, we attempted to calculate the performance index of Rollo and Schulz (*3–6*), to learn whether or not the value of the index is in agreement with the visual evaluation of phantom and clinical images. For this purpose the modified Rollo phantom and Anger focal photon-deficient phantom were made and imaged with two collimator systems.

Received June 3, 1980; revision accepted Aug. 19, 1980.

For reprints contact: Hiroyuki Shinohara, PhD, Dept. of Radiology, Fujigaoka Hospital, Showa Univ., 1-30 Fujigaoka, Midori-ku, Yokohama-shi, 227 Japan.

MATERIALS AND METHODS

The images were made with a 20% energy window, using Searle LFOV 300-keV and 360-keV collimators, here coded "LF-300" and "LF-360", respectively. The physical data for each collimator are shown in Table 1 of Ref. 7. The LF-300 gives higher sensitivity than does the LF-360, but in spatial resolution the latter is superior. The difference is ascribable to the collimators' hole lengths. The relative contributions of the Ga-67 peaks were measured without collimator by recording the count rates produced by a small Ga-67 source in a 10 × 10-cm square on the crystal face, at a distance of 1.5 m. The other parts of the crystal were covered with a lead shield

TABLE 1. SEARLE LFOV COLLIMATOR SPECIFICATIONS

	LF-300*	LF-360*
Max energy (keV)	300	360
Hole geometry	square	square
Hole eff. diameter (mm)	3.8	3.8
Center hole length (mm)	49.5	62.8
Septum thickness (mm)	1.32	1.32
Number of holes	5,200	5,200
Sensitivity†	0.88	0.56
System resolution (mm)‡	7.6	6.8

* "LF-300" refers to the Searle large-field-of-view, 300-keV, parallel-hole collimator; "LF-360" is the large-field, 360-keV, parallel-hole collimator.

† Relative to low-energy, all-purpose collimator (LEAP 140 keV).

‡ For Tc-99m at collimator face.

2 cm thick. The relative counts for the Ga-67 peaks with the collimator-detector systems were evaluated with a flood source, 10 × 10 × 1.5 cm, filled with Ga-67 solution.

The line spread function (LSF) of each detector system was measured by placing a plastic catheter, 1 mm inner diameter and containing Ga-67, under a collimating slit made of two lead bricks 5 cm thick. The slit was 1.5 mm wide and 10 cm long. The LSF of the collimator-detector system was measured by positioning the line source in the center of collimator. The resulting photographic density distribution in the image was scanned by a microphotometer,* with 250-μm slit width and 2500-μm slit height, interfaced to a minicomputer. The digitized photographic density was converted to LSF

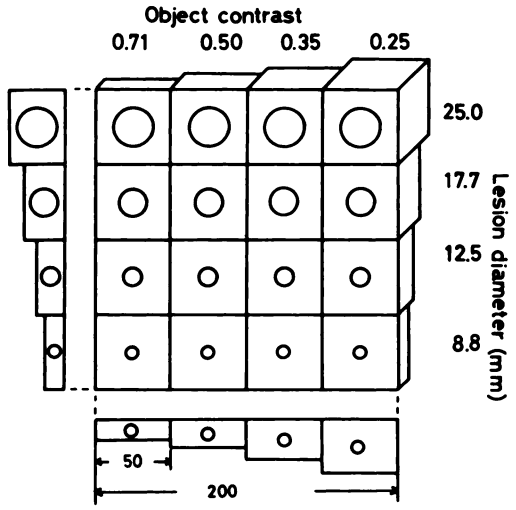

FIG. 1. Design of modified Rollo phantom used to calculate contrast efficiency functions. Side view shows how depth of each sphere is varied to provide varying object contrast.

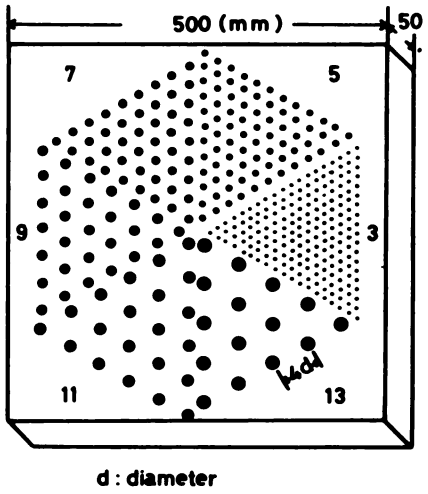

FIG. 2. Anger phantom consists of steel cylinders with various radii surrounded by solution of Ga-67.

on the basis of a characteristic curve.

Figures 1 and 2 show drawings of the modified Rollo phantom and Anger focal photon-deficient phantom.

RESULTS

The relative counts in the Ga-67 peaks with and without collimator (collimator-detector system) are shown in Fig. 3, where the 93-keV peak is taken as a standard. It is readily seen that, relative to the 93-keV peak, only the 300-keV peak (C) shows much change between the two types of collimation, the relative fraction of 300-keV photons being much greater for LF-300 than for the LF-360. The obvious interpretation is that both collimators have relatively more septal penetration by the 300-keV photons than by the two lower energies, and that this penetration is worse with LF-300 than with the LF-360. With regard to sensitivity, the LF-300 is about 1.6 times as sensitive as LF-360.

Figure 4A shows intrinsic spatial resolution in terms of MTF, while the system spatial resolutions are given

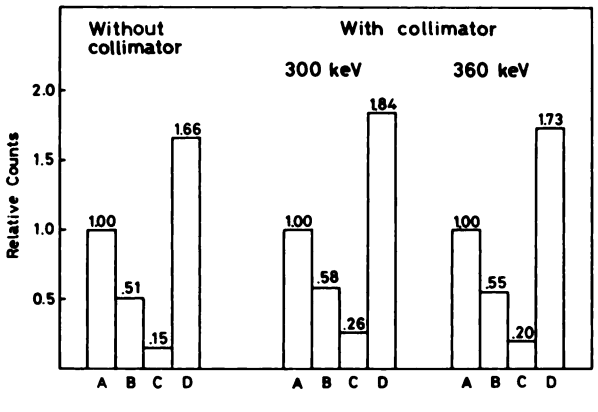

FIG. 3. Relative counts of Ga-67 peaks with or without collimator (collimator-detector system), where the 93-keV peak is taken as standard. A, B, C, and D symbolize 93, 185, 300 keV peak and triple peaks.

in Figs. 4B and 4C. The MTF for a single peak tends to show higher values with increase in photon energy, but note that the MTF for a triple-peak system (D) shows lower values than that for the 93-keV peak.

Rollo et al. (*3–6*) developed the concepts of a contrast efficiency function, Ec(r), and a performance index, PI(r), which measure how an imaging system detects a spherical void of activity, of radius r, within an activity distribution. These indices are calculated as follows:

$$Ec(r) = \frac{C_i(r)}{C_o(r)}$$

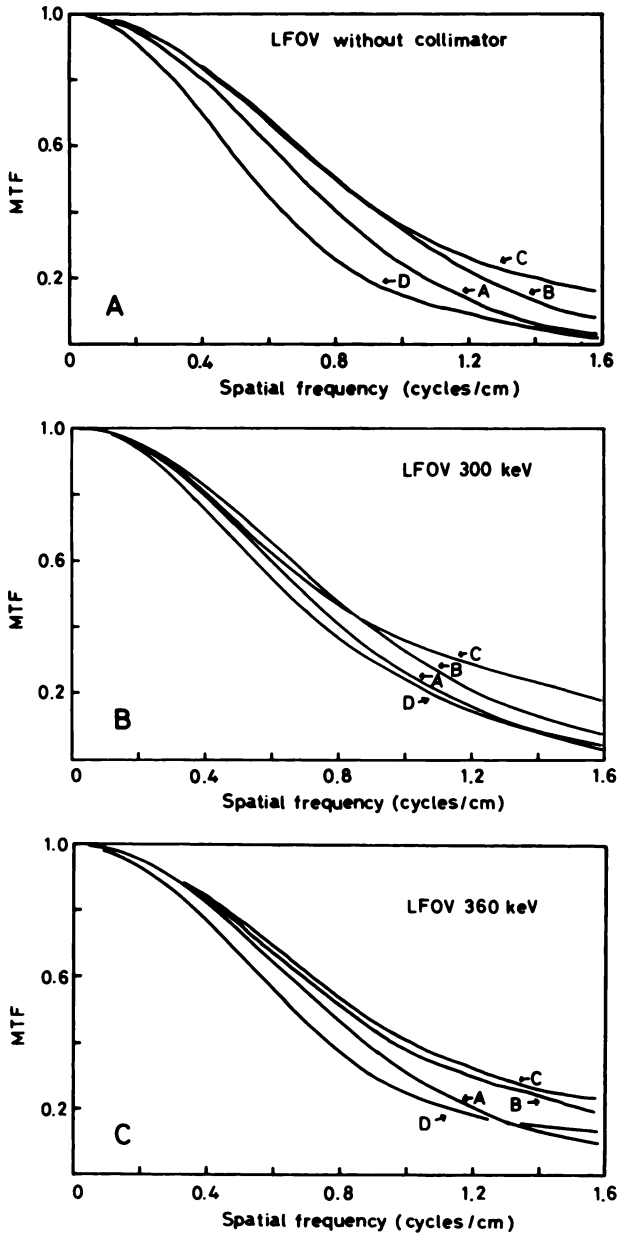

FIG. 4. Top: intrinsic spatial resolution, expressed as MTF, of LFOV with 20% energy window for each of three Ga-67 peaks and the triple window. Middle: spatial resolution of LFOV 300-keV collimator with 20% energy window. Bottom: LFOV 360-keV collimator. For symbols A–D, see legend of Fig. 3.

where $C_o(r)$ = object contrast of the modified Rollo phantom; and $C_i(r)$ = image contrast, calculated as:

$$\frac{\text{(cell background} - \text{void activity)}}{\text{cell background}}.$$

The performance index is then calculated as $PI(r) = Ec(r)\sqrt{S}$, where S = plane sensitivity.

In Figs. 5A–5D, contrast efficiency functions and modulation transfer functions for Ga-67 peaks are compared for the two collimator systems. Large spherical lesions correspond to low spatial frequencies, whereas small spherical lesions correspond to high frequencies; therefore Ec approaches 1 with an increase in lesion radius, as is expected from Eq. A-4 (Appendix). As a matter of convenience, the same numerical values are used in the scales for Ec and MTF in Figs. 5A–5D, although these numbers represent reciprocal units (cm and cm^{-1}) so that the two sets of curves, though measuring similar effects go in opposite directions.

If one compares the Ec curves of the two collimator systems for lesions having radii between 4.4 and 12.5 mm (minimum and maximum lesion radii in Fig. 1), clear differences are evident in the 93 or 300-keV peaks, whereas the difference in Ec values is reduced in the case of the 185-keV peak. Thus regarding the detection of photon-deficient lesions, Ec indicates a collimator's performance better than MTF. With regard to triple peaks (Fig. 5D) compared with a single peak, better spatial resolution is obtained with LF-360, especially using the 300-keV peak.

The overall performance of a collimator-detector system, including spatial resolution and sensitivity, was estimated by the performance index, and the results are plotted in Fig. 6. These curves were generated using the Ec curves for triple peaks in Fig. 5D and adjusting for collimator sensitivity (LF-300/LF-360 = 1.6). When the factor of random fluctuation is included in evaluating system performance, LF-300 is superior to LF-360 for the detection of photon-deficient lesions. From the physical evaluation derived from the PI, we conclude that LF-300 is preferable for Ga-67 imaging, although in spatial resolution it is inferior to LF-360.

Figure 7 shows the behavior of PI for the two collimators, with single peak and the triple-peak window. The value for S in the equation for PI is derived from the relative counts in the Ga-67 peaks in Fig. 3. In Fig. 6 the PI curves include the different collimator sensitivities but the Fig. 7 curves do not; therefore the triple-peak curves for LF-300 and LF-360 are different in Fig. 6 but are about the same in Figs. 7A and 7B (see Fig. 3). The advantage of using three peaks is chiefly the high relative count rate in comparison with that for a single peak. The images in Fig. 8 were made with triple peaks.

The lesion-detecting of the two collimators is compared by imaging the modified Rollo phantom with equal accumulation times (Fig. 8). The observers were one

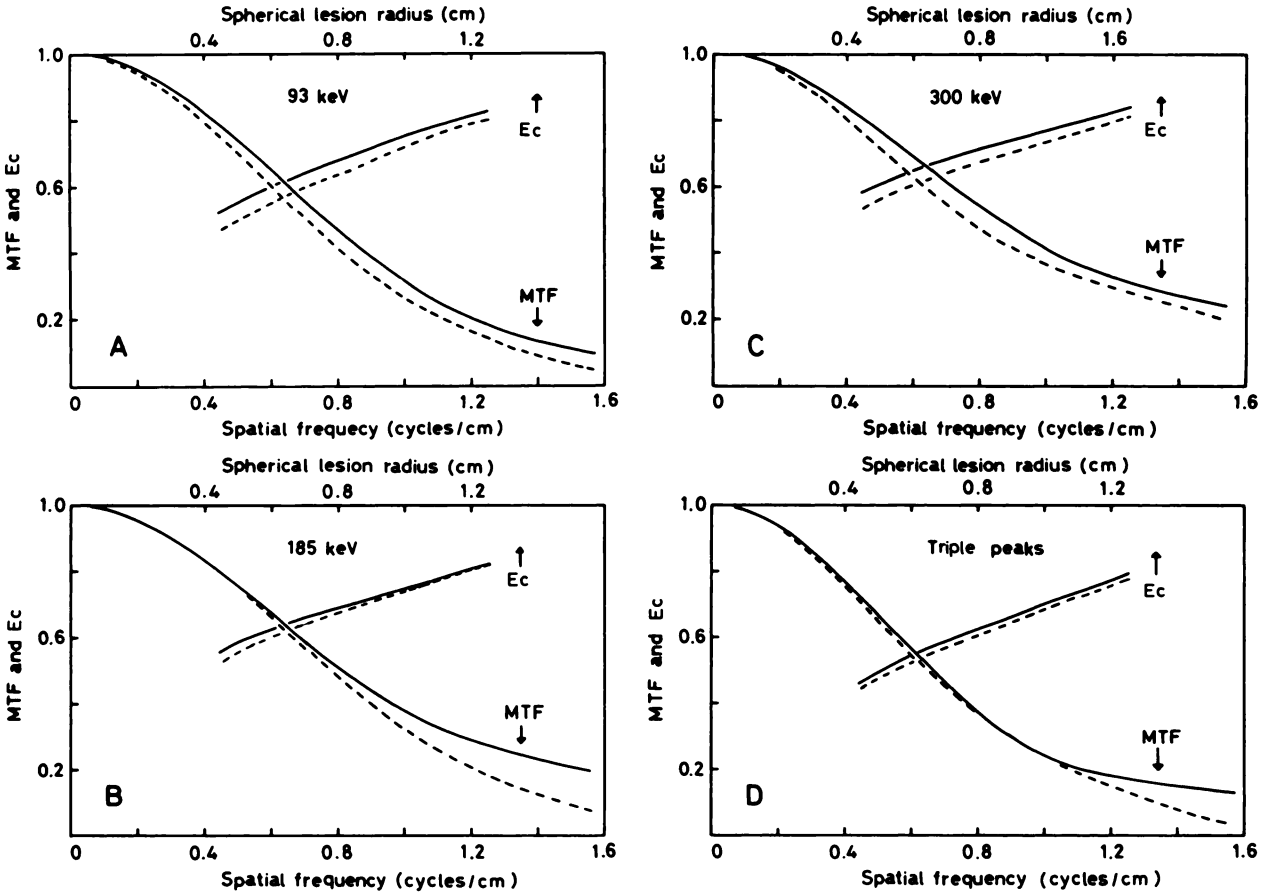

FIG. 5. Contrast efficiency functions, EC, for Ga-67 peaks. Solid line represents 360-keV collimator; dotted line the 300-keV collimator. Symbols A–D as in Fig. 3.

physicist and three technologists with two or more years of experience in nuclear medicine. The observers indicated their level of confidence according to the following scale: 4 = confidence approaching 100% that a lesion is present; 3 = less confidence (~75%) that a lesion is present; 2 = ~50% confidence; and 1 = lesion only suspected, confidence minimum (~25%). The detection tests were repeated three times and the average value for level of confidence was calculated. Lesion detectability is estimated as

$$LD = \frac{\text{Sum of detected photon-deficient lesions}}{\text{Number of photon-deficient lesions in phantom } (=16)} \quad (1)$$

It was tentatively calculated for three levels of confidence (4, 4+3, and 4+3+2) and the results are summarized in Fig. 9.

Clearly the ability of the two collimators in detecting photon-deficient lesion is dependent on the count density obtained in a given imaging time. We find that if count densities in the range of 1000 counts/cm^2 over the liver cannot be achieved by LF-360 in a reasonable imaging time, LF-300 may be more effective by decreasing random fluctuation, leading to better lesion detectability. On the other hand, if the random fluctuation is relatively low because of an increase in count density, LF-360 gives

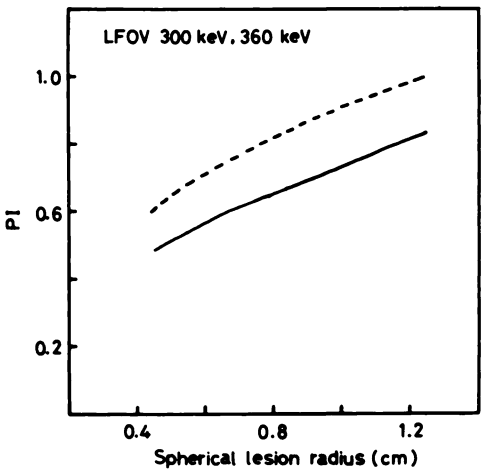

FIG. 6. Comparison of performance index (triple peaks) for the 300-keV collimator (dotted line) and 360-keV collimator (solid line).

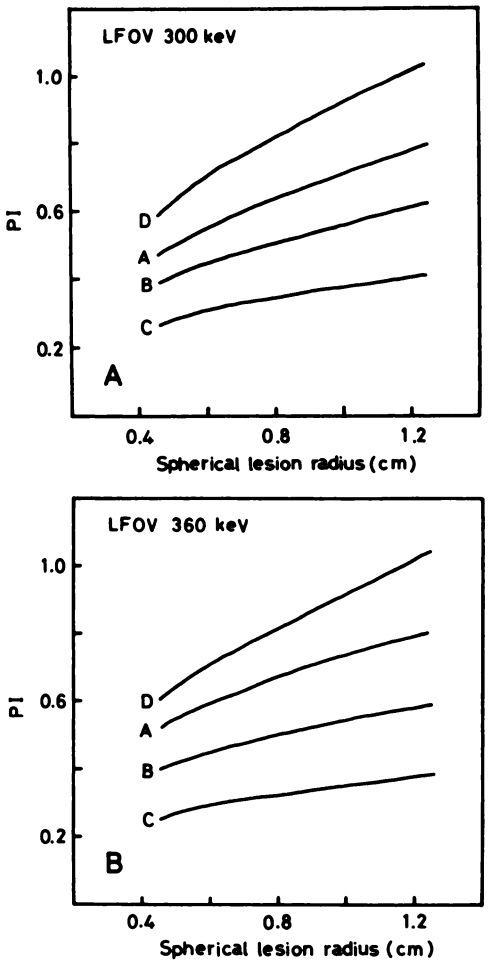

FIG. 7. Comparison of performance index for each single peak of Ga-67 with that for triple peaks. Left: 300-keV collimator; right: 360-keV collimator. Symbols A–D, as in Fig. 3.

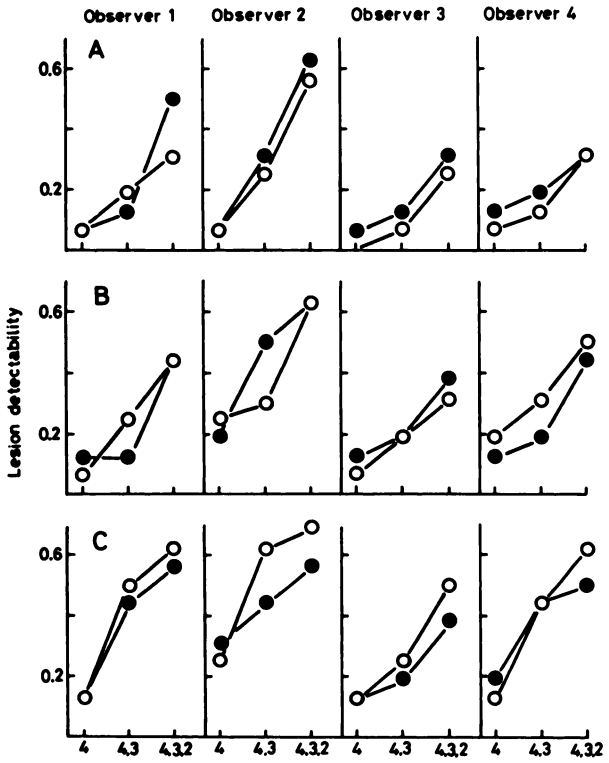

FIG. 9. Lesion detectability for the four observers, at various confidence levels, calculated by Eq. 1. O: 360-keV collimator. ●: 300-keV collimator. A: count densities for the 300-keV and 360-keV collimators are 800 and 500 counts/cm^2, respectively; B: similarly 1600 and 1000 c/cm^2; C: 3200 and 2000 c/cm^2.

better lesion detection than LF-300, which might be deduced from the contrast efficiency function.

Figure 10 shows images of the Anger focal photon-deficient phantom taken with equal accumulation times. In the photon-deficient areas with diameters of 11 and 13 mm, the edge of circle is clearer with LF-360. On the other hand, LF-300 is better for the detection of photon-deficient areas 5 mm in diameter, although the difference is trifling. This finding indicates that higher count densities will be required for the detection of focal photon-deficient regions with smaller diameters. From the visual evaluation of these images, we conclude that image quality with LF-360 is slightly superior to that with LF-300, although this is dependent on count density.

To determine whether or not the visual evaluation based on the phantom images is applicable to clinical Ga-67 imaging, scintigrams were made on the same patient with LF-300 and LF-360 (Fig. 11). Although the difference is too subtle for a claim that a single pair of images demonstrates clear superiority of a collimator, the images suggest that the edge of a focal defect shows up slightly better with the LF-360, as is also indicated by the lesion detectability observed in Fig. 9, B or C.

DISCUSSION

The present work concerns the selection of a collimator for Ga-67 imaging with a triple window. Although

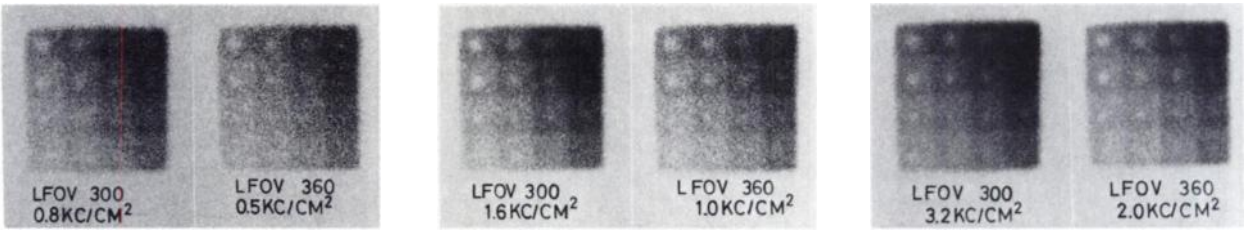

FIG. 8. Images of modified Rollo phantom with two collimators using equal accumulation times.

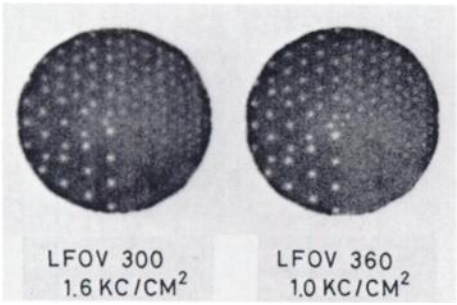

FIG. 10. Anger "focal photon-deficient" phantom images with the two collimators, taken for equal data accumulation times.

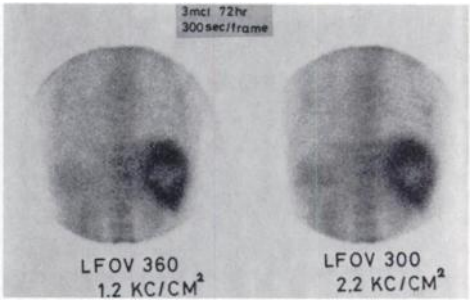

FIG. 11. Clinical Ga-67 images with focal defect in liver, obtained from same patient at 72 hours after injection. Edge of defect is slightly clearer with 360-keV collimator.

comparison of single-window with multiple-window imaging should be studied further, we may infer from Fig. 4A that triple-window imaging is inferior to single-window imaging in spatial resolution. Before this experiment the camera underwent a weekly or daily quality-control program in which the adjustment of Ga-67 photopeaks was made by the manufacturer. We therefore consider that the camera's performance is satisfactory for diagnostic imaging and that the observed MTFs in Fig. 4A [MTF for triple peaks (D) < MTF for 93-keV peak (A)] is not due to faulty quality control but to intrinsic performance of the scintillation camera with triple window (Searle LFOV). A likely explanation for the poorer MTF for triple peaks is the lack of perfect alignment of line-source images for the different energies produced by the ratio circuits of the camera. Ideally the MTF for triple peaks should be equal to the sum of MTFs for single peaks, multiplied by the relative count factor from Fig. 3, and in such a case at least, the MTF for triple peaks should not be lower than that for the 93-keV peak. If the adjustment of photopeaks is distorted under daily usage, Ga-67 image quality with three peaks becomes that much worse. The adjustment responsible for the degradation of spatial resolution is beyond a user's scope of maintenance and dependent on the manufacturer. It is preferable to include the measurement of spatial resolution expressed as LSF or MTF among quality-control programs for a scintillation camera with triple window. These daily or weekly checks will assist the user in the detection of minimal changes in camera performance at the earliest possible date.

Our visual evaluation of the two collimators was based on the lesion detectability assumed in Eq. 1. In practice, three copies of each image in Fig. 8 ($6 \times 3 = 18$) were made and these 18 images were randomly displayed on a screen. Four observers then decided whether or not they could see the lesions, viewed from a distance of 1.5 m. The observer, of course, did not know whether the image displayed on the screen was taken with the LF-300 collimator or LF-360. We concede, however, that our observer study is not as valid as an ROC analysis (*8–10*), because the observer knows ahead of time that 16 spherical lesions are present in the image regardless of his perception. Therefore it is hard for him to say, without prejudice, whether or not he can see a defect. The main difference between the two analyses becomes manifest for holes with small radii and low object contrast. If a lesion falls below a 50% level of confidence an observer's opinion may be influenced by his knowledge that the lesion is there anyway, and also because it and surrounding lesions form a regular progression toward invisibility. This perhaps gives a higher true-positive fraction compared with that obtained in an ROC analysis. On the other hand, a lesion with larger radius and better contrast might well be detected with >75% confidence even if the observer had not known beforehand that it was there. The present analysis, therefore, is inevitably dependent on the assumption of unbiased observers except when they deliver a large true-positive fraction in their detection tests. If this assumption is permissible, the consistency of observer performance seen in Fig. 9 does give our conclusions some credibility. Hoffer (*2*) mentioned qualitatively that a collimator suitable for imaging I-131 (364 keV) is suitable for Ga-67 imaging. Our findings support his idea.

Practical Ga-67 imaging more often involves the detection of lesions with increased activity, whereas the present experiments are related to the detection of photon-deficient lesions. It is admitted, however, that the former is usually easier than the latter (*6*). Therefore the result obtained here may be pertinent to clinical Ga-67 imaging.

In the original Rollo phantom, 16 spherical lesions are situated at equal distances from the upper and lower surfaces, so it is symmetric with respect to the axis connecting the spherical lesions having the same radius. These are not similarly situated in the modified phantom, in order to include different scattering effects depending on which surface faces toward the detector. Thus in the modified phantom the distance between a spherical lesion and detector varies along with the object contrast (Fig. 1). In a strict sense, the same MTF cannot be used in calculating the contrast efficiency function for spherical lesions with different radii, but Figs. 5A–5D may still be useful because we are not concerned with the absolute value of the contrast efficiency function but with

its difference between the two collimator systems.

According to Rollo et al., lesion detectability is primarily a function of four parameters: spatial resolution, object contrast, count density, and lesion size (*6*). Images with the LF-300 or LF-360 collimator in Fig. 8 were compared at three different count densities. In order to investigate a correlation between the performance index and visual evaluation in detail, radionuclides other than Ga-67, giving different count densities, may need study. These experiments are now under way.

CONCLUSIONS

Gallium-67 images taken with equal accumulation times were compared, using two collimators, in terms of physical or visual evaluation. The 300-keV collimator was recommended by the physical evaluation, but lesion detectability derived from the visual evaluation of images from the modified Rollo phantom supported the 360-keV collimator if a count density >1000 counts/cm^2 could be achieved in a reasonable imaging time. In accordance with the phantom images, a clinical Ga-67 image should be slightly superior with the 360-keV collimator than with the 300-keV collimator.

FOOTNOTE

* Sakura PDS 15.

APPENDIX

Measurement of LSF. The digitized photographic density distribution for the line source is converted to LSF on the basis of a characteristic curve as follows. Twenty photographic- and count-density data (x_i, y_i; $i = 1 \sim 20$) are chosen from the characteristic curve and stored in the memory of the minicomputer. If a scanned photographic density, x, falls within the range, $x_1 < x \leq x_5$, the corresponding count density, y, is calculated by the fourth degree of a Lagrange interpolation as is shown in Eq. A-1 (x_i, y_i; $i = 1 \sim 5$ are used). If the x satisfies the condition, $x_5 < x \leq x_{10}$, the values (x_i, y_i; $i = 6 \sim 10$) are used in Eq. A-1 and so on.

$$y = y_1 \frac{(x - x_2)(x - x_3) \cdots (x - x_5)}{(x_1 - x_2)(x_1 - x_3) \cdots (x_1 - x_5)} + \cdots + y_5 \frac{(x - x_1)(x - x_2) \cdots (x - x_4)}{(x_5 - x_1)(x_5 - x_2) \cdots (x_5 - x_4)} \quad \text{(A-1)}$$

If one chooses an arbitrary photographic density, a comparison between the count density calculated from Eq. A-1 and the one read from the characteristic curve shows fairly good agreement.

In an investigation of the effect of LSF sampling distance on computed MTF, it is useful to begin by representing the line spread function by a simple analytic function whose Fourier transform is known in closed form, since the true transfer function can then be predicted analytically. It is well known that if the scattering effect is not significant, the LSF can be approximated by a Gaussian function whose Fourier transform is also Gaussian. Gaussian functions with different d values (see Eq. A-2, below), are transformed in the Simpson rule approximation by varying sampling distances in order to compare the obtained values with those given analytically by Eq. A-3. From the result, a practical LSF sampling distance is chosen in the range of 0.1 mm, which does not cause a significant error in the calculated MTF.

$$f(x) = \sqrt{\frac{2.773}{\pi d}} \exp(-2.773x^2/d^2), \quad \text{(A-2)}$$

where d = full width at half maximum (FWHM);

$$f(u) = \exp(-3.559d^2u^2), \quad \text{(A-3)}$$

where u = spatial frequency.

Contrast efficiency function. Ec(r) was calculated from Eq. A-4, developed by Rollo et al.

$$Ec(r) = \frac{C_i(r)}{C_0(r)} = \frac{\int fL(f)MTF(f)df}{\int fL(f)df}, \quad \text{(A-4)}$$

where f is the spatial frequency and MTF(f) the modulation transfer function. L(f) is the transfer function for any spherical lesion having radius r, and is found as follows:

$$L(f) = \frac{3\sin(2\pi fr)}{(2\pi fr)^3} - \frac{3\cos(2\pi fr)}{(2\pi fr)^2} \quad \text{(A-5)}$$

This function is derived as follows. Let us consider the following function:

$$h(r) = \begin{cases} 0 & |r| > a \\ 1 & |r| \leq a \end{cases} \quad \text{(A-6)}$$

Its normalized three-dimensional Fourier transform is

$$H(f) = \frac{\int_{-\infty}^{\infty}\int_{-\infty}^{\infty}\int_{-\infty}^{\infty} h(r)e^{-i2\pi f \cdot r}dv}{\int_{-\infty}^{\infty}\int_{-\infty}^{\infty}\int_{-\infty}^{\infty} h(r) \cdot dv} \quad \text{(A-7)}$$

The numerator of Eq. A-7 is rewritten by using the spherical polar coordinates r, θ, φ.

$$dv = r^2(\sin\theta) \cdot d\theta \cdot d\phi \cdot dr$$
$$f \cdot r = fr\cos\theta. \quad \text{(A-8)}$$

The denominator of Eq. A-7 is simply a volume of sphere having radius a and is given by $\frac{4}{3}\pi a^3$.

$$H(f) = \frac{\int_0^a \left[\int_0^{\pi} \left\{\int_0^{2\pi} h(r) \exp(-i2\pi fr\cos\theta) \cdot d\phi\right\} \sin\theta \cdot d\theta\right] r^2 \cdot dr}{\frac{4}{3}\pi a^3} \quad \text{(A-9)}$$

and thus Eq. A-5 is obtained.

REFERENCES

1. HOFFER PB, SCHOR R, ASHBY D, et al: Comparison of Ga-67 citrate images obtained with rectilinear scanner and large-field Anger camera. *J Nucl Med* 18: 538-541, 1977
2. HOFFER PB: Gallium-67 Imaging, Hoffer PB, Bekerman C, Henken R. eds. John Wiley & Sons, New York, 1978, p 9
3. ROLLO FD, SCHULZ AG: A contrast efficiency function for quantitatively measuring the spatial-resolution characteristics of scanning systems. *J Nucl Med* 11: 53-60, 1970
4. ROLLO FD, SCHULZ AG: Effect of pulse-height selection on lesion detection performance. *J Nucl Med* 12: 690-696, 1971
5. ROLLO FD: An index to compare the performance of scintigraphic imaging systems. *J Nucl Med* 15: 757-762, 1974

6. ROLLO FD, HARRIS CC: Nuclear medicine physics, instrumentation, and agents, Rollo FD. ed. The C. V. Mosby, Missouri, 1977, p 387
7. Searle Radiographics: Operation mannual for Pho/Gamma LFOV standard model 6478 or operator's console model 3204
8. GOODENOUGH DJ, ROSSMANN K, LUSTED LB: Radiographic applications of receiver operating characteristic (ROC) curves. *Radiology* 110: 89-95, 1974
9. GREEN DM, SWETS JA: *Signal Detection Theory and Psychophysics.* (rev. ed). Huntington, NY, Krieger, 1974, pp 99-106
10. METZ CE: Basic principles of ROC analysis. *Semin Nucl Med* 8: 283-298, 1978